CLM - P 176





CLM - P 176



United Kingdom Atomic Energy Authority

RESEARCH GROUP

Preprint

# A SPECTROSCOPIC STUDY OF THE PLASMA GENERATED BY A LASER FROM POLYETHYLENE

B. C. BOLAND
F. E. IRONS
R. W. P. McWHIRTER

Culham Laboratory
Abingdon Berkshire

1968

UNCLASSIFIED
(Approved for publication)

CLM - P 176

# A SPECTROSCOPIC STUDY OF THE PLASMA GENERATED BY A LASER FROM POLYETHYLENE

by

B.C. BOLAND
F.E. IRONS
R.W.P. McWHIRTER

(Submitted for Publication in J. of Phys. B. (Proc. Phys. Soc.)

## ABSTRACT

This paper describes a spectroscopic study of the plasma produced when a giant pulse ruby laser beam of 5 joules energy and 17 nanoseconds duration is focussed into a 0·3 mm diameter spot on a polythene target in vacuum. Quantitative measurements of spectral intensities in the range from 20Å to 6000Å have yielded estimates of the electron and ion densities, the electron temperature and the streaming velocities of the ions. From these results it is estimated that the electron temperature, the ionization energy, the energy lost by radiation, and the energy of recoil of the target account for only about 10% of the incident laser energy. The ion kinetic energy accounts for 70% of the incident energy with an experimental uncertainty of ± 70%. It is calculated that there are about $10^{16}$ ions produced by the laser beam striking the target. It is shown that the electrons contained in the plasma expanding away from the target cool adiabatically. In the course of the work there have been identified several new lines hitherto unclassified.

Astrophysics Research Unit, S.R.C.,
Culham Laboratory,
Abingdon,
Berks.

May, 1968

C O N T E N T S

## 1. Introduction

When the radiation from a laser of sufficiently high power is focussed onto a solid target, a plume of luminous plasma is formed. Observations have shown that this luminous plume expands away from the target surface with velocities up to $10^7$ cm $sec^{-1}$ (a few keV of energy). In the spectrum of these plumes the observation of both continuum and line radiation has been reported. (A list of references to earlier spectroscopic work is given separately at the end). The continuum comes from near the target surface and covers most of the spectral range from 20 Å to 6000 Å. From the shape of the continuum spectrum in the vacuum untraviolet region, temperatures up to about 100 electron volts have been estimated. The line spectrum shows high ionization stages of ions and has been recorded out to several centimetres from the target surface. Many new line identifications have resulted from this work.

This paper describes some quantitative spectroscopic measurements and their interpretation, made on the plasma produced when focussed laser radiation falls on a polyethylene foil. Polyethylene was chosen as a convenient material, containing an element (carbon) of suitably low atomic number. Plasma temperatures, densities and directed energies are determined from the spectra and used to build up a model for the mechanism of formation of the plasma. The slope of the free-bound continua of carbon V and VI in the wavelength region between 20 Å and 40 Å was measured to determine the electron temperature as a function of distance from the target surface. Line intensity ratios were used to determine the temperature of the less luminous regions of plasma. Absolute measurements of visible and

near ultraviolet spectral lines representative of all the ions of carbon were made as functions of both time and position in the plasma plume. After showing that the Saha-Boltzmann equation was applicable to the upper levels of these ions the line intensities were interpreted in terms of the densities of the corresponding ions. The same measurements were used to derive values for the kinetic velocities of the ions as they streamed away from the target. It was shown that the total kinetic energy of the ions was about 70% of the original laser energy. During the course of the work, several new lines of C V and VI have been identified.

## 2. Experimental Arrangement

A Korad K1500 ruby laser was used and was operated to give an output of 5 J in the pulse of duration at half maximum of 17 nano seconds. The laser beam passed first through a quartz plate from which a small fraction of the power was reflected onto two diodes (type ITT FW114). The output from one of the diodes provided an oscilloscope trigger; the output from the other, which had been previously calibrated against a TRG 170 calorimeter, placed in the main laser beam, was displayed on an oscilloscope and provided a monitor of laser power. After passing through the quartz plate the laser beam was focussed into a vacuum chamber at $10^{-4}$ torr by a lens of focal length 10 cm, so as to fall normally onto the surface of a polyethylene $(C_2H_4)_n$ foil, 250μ thick. From measurements of the divergence of the beam it was estimated that 70% of the laser power is focussed within a circular spot of diameter 0·3 mm, giving an average light flux of $2{\cdot}9 \times 10^{11}$ watts $cm^{-2}$. The polyethylene foil was wound from a spool inside the vacuum chamber between two pairs of

rollers to locate the target surface to about 0·1 mm.

The axis through the centre of the focal spot at right angles to the target surface and along the central axis of the laser beam will be referred to throughout this paper as the x-axis. The target surface corresponds to the point x = 0.

## 3. Photography of the Spectrum

The spectra shown in figure 1 cover the wavelength range 20-6000 Å, and were recorded with a 2 metre grazing incidence spectrograph (a 10 shot exposure on Q2 plate), a 1 metre normal incidence spectrograph (a 30 shot exposure on Q2 plate), and a Hilger medium quartz spectrograph (a 10 shot exposure on HPS plate). In each case the direction of observation was a right angles to the laser beam and the spectrograph slit was aligned along the x-axis so that the spatial resolution seen in these spectra represents spatial resolution along the x-axis. Spatial resolution was achieved in the case of the grazing incidence spectrograph by a pinhole technique, in the case of the normal incidence spectrograph by positioning the target at the Sirk's focus, and in the case of the medium quartz spectrograph by using a quartz-lithium fluoride achromat.

In the grazing incidence spectrum the resonance line series and recombination continua of C VI and V are clearly seen in many orders. The normal incidence and quartz-visible spectra show continuum and lines of hydrogen and carbon of all stages of ionization. The continuum intensity is greatest at the target surface, and decreases rapidly within a few millimetres of the surface. Some lines show strong Stark broadening near the target surface. Lines of H I and C I and II can be seen at the rear of the target foil. Besides the

lines of hydrogen and carbon which are seen in emission, on one occasion when a titanium doped polyethylene target was used, lines of Ti I were seen in absorption, but lines of Ti II and higher ionization stages were in emission.

### 3.1 Line Identification

Lines have been identified as belonging to hydrogen and carbon of all stages of ionization, with some very weak lines of oxygen and calcium. About 3% of the lines remain unidentified, the strongest of which is at 3526·7 ± 0·5 Å. This line has a time history similar to that of lines of C V and it has been tentatively identified as the transition C V $2s\,^1S - 2p\,^1P$. The identification of lines of the series $2p\,^1P - nd\,^1D$, $2s\,^3S - np\,^3P$ and $2p\,^3P - nd\,^3D$ has already been reported (Fawcett and Irons, 1966). The new identification in Table 1 correspond to transitions amongst the states n = 3 to 9 of C V and VI. These lines are both Stark and Doppler broadened and this broadening limits the accuracy of the wavelength determination.

Table 1

Observed Transitions

| C V | | C VI | |
|---|---|---|---|
| Wavelength | Transition | Wavelength | Transition |
| 4944·7 ± ·5 | 6 - 7 | 3139 | 7–9 |
| 2982·2 ± ·5 | 5 - 6 | 5291 | 7–8 |
| 718·8 ± ·2 | $3p\,^3P - 4d\,^3D$ | 3434 | 6–7 |
| 760·4 ± ·2 | $3p\,^1P - 3d\,^1D$ | 2070·3 | 5–6 |
| 748·4 ± ·2 | $3d\,^3D - 4f\,^3F$ | 728·9 | 4–6 |
| | $3d\,^1D - 4f\,^1F$ | 1124·9 | 4–5 |
| 765·4 ± ·2 | $3p\,^3P - 4s\,^3S$(?) | 520·6 | 3–4 |

The identification of the lines of C V at λ = 718·8 and 760·4 Å is based on an agreement in wavelength with the values calculated from values of the term (n,l) energies (Fawcett and

Irons, 1966). The line at $\lambda = 748{\cdot}4$ Å, identified as it is, gives a value for the energy of the substate 4f equal to that of 4d, within experimental limits, for both triplet and singlet sequences. The line at $\lambda = 765{\cdot}4$ Å appears to belong to the same multiplet as the other lines around this wavelength, and the indicated transition is the member most likely to give a line of this intensity. The identification with C V of the lines at 4944·7 and 2982·2 Å is based on a similarity of their time histories with that of another line of C V (at 2279 Å), and also on the fact that their wavelengths fall within 1 Å of those predicted for the 6-7 and 5-6 transitions of the hydrogen-like ion with atomic number five. Transitions between terms f,g,h and i contribute to the intensities of these lines - the term energies were calculated by interpolation between those of p and d (from Fawcett and Irons, 1966) and h and i (from the hydrogen-like formula). The line corresponding to the transition 4–5 is blended with another line.

The C VI identifications have been made on the grounds that the observed wavelengths are coincident with those predicted (Garcia and Mack, 1965). The time histories of those lines which could be observed photoelectrically ($\lambda\lambda$ 5291, 3434 and 2070 Å) were seen to be similar, and to form a time sequence with lines of C I–V in a way which indicates that they belong to a higher stage of ionization than C V (see later in figure 3).

## 4. The Free-bound Continua of C VI and C V - Measurement of Electron Temperature

In figure 1, in the wavelength range 20–35 Å, can be seen the continua resulting from free-bound transitions onto the ground states

of C VI and V, spatially resolved in the x direction. The spatial resolution, of about 0·5 mm, was achieved by stopping down the length of the entrance slit. A spectrogram was recorded with a 20 shot exposure, sufficient to give a record of the continuum out to x = 2 mm. The spectrogram was scanned with a microdensitometer at several settings parallel to the direction of wavelength dispersion, and plate density was converted to intensity from a knowledge of the instrument calibration, due to Morgan et al., 1968, a correction being made for the overlap of the C VI continuum by the C V continuum.

The free-bound continuum intensity $I_\lambda$ (power/unit area/unit wavelength interval/sterad.) is given by:

$$I_\lambda = \frac{2^7\pi^4 e^{10} m \quad g}{3\sqrt{3} c (2\pi m)^{3/2} h^2} \times \frac{z^4 \, n_e \, n(C^{z+}) \exp\left(\frac{\chi}{kT_e}\right) \quad \exp\left(-\frac{hc}{\lambda kT_e}\right)}{\lambda^2 \, T_e^{3/2}} \times \text{plasma depth} \qquad \ldots (1)$$

where $\chi$ is the ionization potential, g is the Gaunt factor (of order unity), $n_e$ and $T_e$ are the electron density and temperature respectively, and $n(C^{z+})$ is the number density of the carbon ion $C^{z+}$ (Elwert, 1954). This formula is relevant to the hydrogen-like ion $C^{6+}$ and there is a further factor of the order of unity which corrects it for the helium-like ion $C^{5+}$. Thus, from equation (1), the spectral distribution of the continuum gives a measurement of $T_e$, and the spatially resolved intensity at a fixed wavelength gives, after allowing for the variation in $T_e$, a measurement of the variation of the product $n_e \, n(C^{z+})$ with x.

The $\log_e$ of the product of the observed intensity and $\lambda^2$ was plotted against $\lambda^{-1}$ and this gave a straight line, from whose

gradient $T_e$ was calculated. The values of $T_e$ determined in this way are plotted in figure 2 as a function of x. At each point of measurement the two values of $T_e$ (from the two continua) were found to be equal to within experimental limits. Over the region x = 0 - 2 mm the temperature decreases from 90-12 eV. Error limits are shown in figure 2. Errors enter into the temperature measurement via the plate calibration and the need to correct for background radiation.

Also shown in figure 2 are measurements of temperature at x = 3·5 and 5 mm made from line intensity ratios. These are discussed later in the paper.

## 5. Time-Resolved Line Intensities

For the time resolved work a 1·5 metre focal length Ebert-mounted monochromator was used to view the plasma at right angles to the x-axis. Radiation from the plasma was focussed by an achromatic lens (lithium fluoride and quartz) onto the entrance slit of the monochromator; the signal at the exit slit being monitored by a photomultiplier (EMI 9594QB) and thence displayed on a Tektronix 519 oscilloscope. The signal display was delayed with respect to the trigger. The rise time of the system was measured to be ~ 3 ns. The signal magnitude at which the system response departed from linearity was determined experimentally for pulses of the duration encountered in the plasma, and was never exceeded during subsequent experiments (a pulsed light source similar to that described by Mackay et al., 1965 was used for this determination). Calibrated filters were used to attenuate the plasma light signal to bring it within the range of recording of the fixed sensitivity oscilloscope.

In order to make absolute intensity measurements, the complete optical system was intensity calibrated by means of a tungsten strip lamp placed at the target position. The continuum emission from the plasma was used to extend this calibration to wavelengths between 3000 and 2000 Å. The target chamber, including the lens, was mounted on a slide so that plasma at any distance x from the target surface could be brought into the field of view of the monochromator. A stop, whose position on the entrance slit could be varied, made it possible for the monochromator to select any point in the plasma at right angles to the x-axis.

5.1 Distribution along the x-Axis

Typical oscilloscope records (for the point x = 2 mm) showing the time history of some of the lines in the table are shown in figure 3. From these and other similar photographs at different positions x the plots shown in figure 4 were derived, where the peak intensity of each line is put equal to unity at x = 2 mm and the variation of each line intensity with x is as shown in the figure. The zero on the time axis is the time of arrival of the laser pulse at the target surface. The spectral lines of the more highly ionized ions are the first to appear and are followed in turn by ions of successively lower stages of ionization. The lines of C VI and V rise to peak values in times comparable with the instrumental value of ~ 3 ns. At x = 2 mm the time profiles of the lines of C VI and V are hardly distinguishable. With increasing x the time duration of each ion species increases, with the exception however of C VI which remains approximately constant. Also with increasing x the time separations of the intensity peaks increase.

The times of the intensity peaks are plotted in figure 5 as functions of x. They fall on approximately straight lines: the velocities corresponding thereto are listed in table 2. Also shown in figure 5 are two curves, representing the time profile of the visible continuum at x = 0 mm, and the time profile of the laser pulse recorded on the same instrument as, and after it had followed the same path as, the plasma radiation.

Table 2

| Line | Transition | Ion to which velocity measurements refer | Velocity cm $s^{-1}$ | K.E. keV | $\frac{K.E}{Z}$ keV |
|---|---|---|---|---|---|
| C VI 3434 | 6 - 7 | $C^{6+}$ | $3{\cdot}3 \times 10^7$ | 6·7 | 1·1 |
| C V 4945 | 6 - 7 | $C^{5+}$ | 3·1 " | 5·9 | 1·2 |
| C IV 2524 | $4d\,^2D - 5f\,^2F$ | $C^{4+}$ | 2·5 " | 3·9 | 1·0 |
| C III 3609 | $4p\,^3P - 5d\,^3D$ | $C^{3+}$ | 1.6 " | 1·6 | 0·5 |
| C II 4267 | $3d\,^2D - 4f\,^2F$ | $C^{2+}$ | 1·0 " | 0·62 | 0·3 |
| C I 2479 | $2p\,^1S - 3s\,^1P$ | $C^{1+}$ | 0·7 " | 0·26 | 0·3 |

In magnitude the velocities in table 2 are comparable with measurements by other authors of luminous velocities and of particle velocities, for pure carbon plasma generated with laser fluxes comparable to that used here (Basov et al., 1966; Gregg and Thomas, 1966; Langer et al., 1966; and Opower and Press, 1966). The question of the identification of the observed luminous velocities with particle velocities is discussed later.

As regards hydrogen, the time profile of the line $H_\beta$ was observed to be similar to that of C I 2479.

It may be noted that most of the radiation emitted by the plasma in the visible region of the spectrum is due to the more weakly ionized species. Hence it might be expected (as was observed

by Basov et al., 1966) that a velocity derived from an undispersed streak camera photograph would be smaller than the maximum velocity.

5.2 Distribution perpendicular to the x-axis

The data in figure 4 can be used to construct the spatial distribution of ion species along the x-axis at set times. Additional observations at right angles to the axis enabled this construction to be extended off-axis, resulting in a two-dimensional map of the distribution of ion species throughout the plasma. Each ion species was observed to be distributed fairly symmetrically about the x-axis, the more highly ionized ions having the smallest spread. The distance apart of the two points either side of the x-axis at which the on-axis intensity of a line falls to half is called the 'plasma depth.' The plasma depth at the target surface is put equal to the depth observed there for the visible continuum.

6. The Interpretation of the Line Intensities

It has been shown that the population density of the upper levels of an ion of charge $z - 1$ present in a plasma is related to the population density of the next ion having charge $z$ and the electron density by the Saha-Boltzmann equation (Bates et al., 1962). In order that this should be so for a particular level it is necessary that the electron density should satisfy the following inequality (McWhirter, 1965).

$$n_e > 1{\cdot}73 \times 10^{14}\ T_e^{\frac{1}{2}}\ \chi(p,q)^3 \qquad \ldots (2)$$

where $T_e$ and $\chi(p,q)$ are in eV. The use of the Saha-Boltzmann equation in this way then leads to the following expression for the intensity of a spectral line as power/unit area/sterad.

$$I = \left(\frac{h^2}{2\pi m\, kT_e}\right)^{3/2} \frac{\omega A h\upsilon}{2\,\omega(C^{z+})\,4\pi} n_e\, n(C^{z+}) \exp\left(\frac{\chi}{kT_e}\right) \times \text{plasma depth} \quad \ldots (3)$$

where, besides the usual symbols, $\omega$ and $\chi$ are the statistical weight and ionization potential respectively of the excited state of the ion $z-1$, and $\omega(C^{z+})$ and $n(C^{z+})$ are the statistical weight and number density respectively of the ground state of the ion $z$. $A$ is the transition probability and values have been taken from the tables due to Wiese et al., 1966, for all lines except C V 4945. For the line C V 4945, $\omega A$ was calculated by the method of Bates and Damgaard, 1949, ( $= 4{\cdot}7 \times 10^{10} s^{-1}$).

6.1 Densities at $x = 2$ mm

We now confine our attention to that point at $x = 2$ mm, where the measurements of $I$ and $T_e$ overlap. The values of $T_e$ measured from the free-bound continua (figure 2) apply to C VI and V, and also to C IV, since radiation from these three ions comes from approximately the same region of plasma. The values of $T_e$ for C III and II were determined from the ratio of line intensities, assuming a Boltzmann distribution. The lines used were $\lambda = 2163$ and 3609 Å for C III, and 3920 and 4267 Å for C II. For the levels from which these lines originate, an estimate of the maximum deviations of population density below the Saha-Boltzmann value was obtained from the tables of McWhirter and Hearn, 1963 and was found to be at most 30%. Allowance was made for this deviation. The value of $T_e$ for C I cannot be measured in this way because of the lack of suitable lines: it can however be put as less than that of C II.

In Table 3 are listed the experimentally determined values of I (peak intensities) and $T_e$, and the values of $n_e\, n(C^{Z+})$ obtained after substitution into equation (3). Shot-to-shot variations and uncertainties in the intensity calibration introduce an error in I of about 20%. The above causes and also the uncertainty in the use of equation (3) introduce the errors into $T_e$ which are shown in Table 3.

Table 3

| Line | I<br>W $cm^{-2}$ $sterad^{-1}$ | $T_e$<br>eV | $n_e n(C^{Z+})$<br>$cm^{-6}$ | $n(C^{Z+})$<br>$cm^{-3}$ |
|---|---|---|---|---|
| C VI 3434 | 70 ± 20% | $12^{+4}_{-2}$ | $1{\cdot}5 \times 10^{34}$ | $0{\cdot}3 \pm {\cdot}2 \times 10^{17}$ |
| C V 4945 | 120 " | " | 11 " | $1{\cdot}2 \pm {\cdot}4$ " |
| C VI 2524 | 82 " | " | $7{\cdot}3$ " | $0{\cdot}8 \pm {\cdot}4$ " |
| C III 3609 | $8{\cdot}3$ " | $4{\cdot}0^{+1{\cdot}5}_{-\ {\cdot}7}$ | $1{\cdot}8 \times 10^{34}$ | $0{\cdot}6 \pm {\cdot}2 \times 10^{17}$ |
| C II 4267 | 46 " | $1{\cdot}9^{+\ {\cdot}9}_{-\ {\cdot}3}$ | $0{\cdot}36$ " | $0{\cdot}3 \pm {\cdot}15$ " |
| C I 2479 | 18 " | < " | $<0{\cdot}75$ " | $<0{\cdot}5 \pm {\cdot}25$ " |

Charge netrality is invoked to obtain individual densities from the products $n_e\, n(C^{Z+})$ and these are shown in the last column of Table 3. The application of charge neutrality is quite straightforward in the case of the ions C I - III since the emission from these ions is separate in time. Radiation from the ions C IV - VI is not separated in time (at x = 2 mm), though an intensity scan at right angles to the x axis shows a slight separation in space, with the C VI emission being concentrated slightly more closely to the axis than is that of C V, which in turn is concentrated slightly more closely than that of C IV. Unfortunately

these scans could not be made with sufficient accuracy on a shot-to-shot basis to warrant an Abel inversion procedure to resolve the various regions of emission. Consequently two limiting distributions were considered, namely than in which all three ions are separated, and that in which all ions occupy the same region of space. The former gives an upper limit to the ion density and the latter a lower limit. These limits, further extended by incorporating experimental errors, are shown in figure 6. Estimates of mean density are given in Table 3.

In applying charge neutrality it has been assumed that hydrogen ions coexist with carbon ions in the ratio 2:1 as in polyethylene. However the majority of the electrons are due to the carbon ions and this assumption is not critical.

A substitution of the above determined densities back into equation (2) showed the inequality therein to be satisfied for each ion. Furthermore, a substitution in the tables of McWhirter and Hearn, 1963, showed that the times taken by the densities of the excited states to relax to their quasi steady state values were several orders of magnitude smaller than times characteristic of the plasma. The use of equation (3) is therefore justified.

### 6.2 Densities in the Region $x < 2$ mm

The variation of the observed free-bound continuum intensity, $I_\lambda$, with $x$ at constant $\lambda$ can be interpreted to give the relative variation of the product $n_e\, n(C^{z+})$ with $x$ (equation (1)). From one spectrogram, recorded with a 20 shot exposure and a spatial resolution of 0·5 mm, a plot of $I_\lambda$ versus $x$ was obtained over the region $x < 2$ mm. From a second spectrogram recorded with only a single shot exposure but an improved spatial resolution of 0·1 mm

a plot of $I_\lambda$ was obtained over the region $x < 0{\cdot}6$ mm (only a single shot exposure because of the difficulty of relocating the target surface to within 0·1 mm). An extension of this latter plot beyond $x = 0{\cdot}6$ mm was made such than when this 'composite plot' was folded with a slit length of 0·5 mm the resultant plot gave the best fit to that observed with the longer slit. This 'composite plot' was substituted into equation (1), along with the measured values of $T_e$ and plasma depth, to give the relative variation of $n_e\ n(C^{Z+})$ with x. For this measurement the intensities of the continuum close to the edges at the series limits were taken. This variation was then made absolute by means of the values of this quantity determined at $x = 2$ mm from absolute line intensities (Table 3). Considerations of plasma composition similar to those described previously then led to a calculation of the mean densities of $n(C^{6+})$ and $n(C^{5+})$ over the region $x < 2$ mm. These are shown in figure 6. Note that it was not possible to do this for $n(C^{4+})$ because the C IV recombination continuum was not observed. The densities at the target surface were found to be $n(C^{6+}) \sim 7 \times 10^{17}$ cm$^{-3}$ and $n(C^{5+}) \sim 1{\cdot}7 \times 10^{18}$ cm$^{-3}$.

Using the above determined values of $n(C^{6+})$ and $n(C^{5+})$ at the target surface, a calculation was made of the absolute intensity of the C VI and V continua in the visible region of the spectrum (assuming that it is mostly optically thin free-free radiation). This was found to be within a factor three of the observed intensity.

### 6.3 Plasma Opacity

Inherent in the interpretation of the free-bound continuum and the line intensities has been the assumption of optical transparency.

Cooper, 1966, and Wilson, 1962, give criteria for the optical transparency of hydrogen-like and non hydrogen-like free-bound continua respectively, and these are readily shown to be satisfied in the present plasma. The criterion given by Cooper, 1966, for the optical transparency of dispersive line profiles is also well satisfied for all the lines considered here, even when maximum values are taken for the population density of the lower level of each transition, i.e. thermal values with respect to the next ionisation stage. The assumption of optical transparency is therefore valid in all cases.

## 6.4 The Determination of the Streaming Velocity of the Various Ions

Before the measured luminous velocities in Table 2 may be identified directly with the velocities of the ions it is necessary to show that recombination does not play an important part. Clearly if the plasma is recombining strongly as it expands, then a particular ion which starts at the target surface as say C VI may very well be observed as an ion of maybe C III at some distance from the target.

From the observed values of temperature and density, calculations have been made of the recombination rates for the ions C IV, V and VI, assuming that the dominant recombination mechanism is that proposed by Bates et al., 1962, (whose tabulated values are used in the evaluation) and based on their collisional-radiative model. These calculations were extended to cover the region x = 2-5 mm by measuring values of $T_e$ from the intensity ratios of two C VI lines at $\lambda$ = 3434 and 5290 Å (see figure 2) and by calculating the values of density from the observed line intensities, as described

previously. These calculations showed that the recombination rate for these ions was sufficiently slow that it had negligible effect in changing the population densities of the ions during their time of flight from x = 1 to 5 mm.

There is also experimental evidence that recombination is not an important process in determining the time and space resolved intensity profiles. The density ratio of $C^{6+}$ to $C^{5+}$ was determined from the ratio of the free-bound continua already referred to and from the ratios of the intensities of lines of C VI and C V. This density ratio is found to be constant from x = 5 to 1 mm and to increase by a factor of two within 1 mm. The fact that the density ratio is constant over such a large distance is a reasonably satisfactory indication that recombination is not a dominant mechanism for these ions.

An estimate has also been made, at the point x = 2 mm of the recombination times for the ions C III and II, using the tables of Bates et al., 1962, for a pseudo-alkali ion. These times are a factor of two longer than the time of expansion to 5 mm.

Thus the values already given in Table 2, are interpreted as the streaming velocities appropriate to the various ions, as the plasma expands out from the target surface. Since the ion masses are known these velocities may be converted to kinetic energies, and these are also shown in Table 2.

The spread in time of the light emission from each ion may now be interpreted as the spread in the ion streaming velocities. The spacing between the numbers in the velocity column of Table 2 gives an indication of the extent of this spread. The distribution of

velocities of the ions leaving a carbon surface after irradiation with a laser pulse of power comparable to that used here has been reported by Langer et al., 1966, and is in fact similar to the distribution of light intensity with time observed here.

It may be noted from figure 5 that the various ions and particularly those of small charge, do not acquire their terminal velocities until some time after the laser pulse is over. This may be alternatively expressed as the lower charge ions continuing to be accelerated for the first few millimetres of their trajectory from the target. This observation is consistent with the view that the acceleration is caused by the formation of a sheath around the plasma. Some idea of the potential developed across this sheath may be given by the figures in the last column of Table 2 where the energy of the ions is divided by their charge.

It may also be noted from figure 5 that, at the target surface, the continuum emission persists from the time of formation of the plasma to the approximate time of appearance of the C I emission.

### 6.5 The Relationship between the Electron Temperature and Density

The electron temperature and the electron density (derived from ion densities of $C^{5+}$ and $C^{6+}$ on the basis of charge neutrality) have been estimated over the region $x = 0 - 2$ mm and are shown plotted, one against the other, in figure 7. Additional points are included in this plot, corresponding to $x = 3{\cdot}5$ and 5 mm. The electron temperature at these points was determined from the ratio of intensities of the C VI lines at $\lambda = 3434$ and 5290 Å, using equation (3), and the electron density from absolute line intensities, as before. The points in figure 7 are best fitted by a law of the

form $T_e\, n_e^{-2/3}$ = constant. Such a law is consistent with the adiabatic expansion of the electron gas.

## 6.6 The Calculation of the Total Number of Ions in the Plasma Plume

By multiplying the measured ion densities in Table 3 with the observed volumes occupied by the ions, the total numbers of ions $N(C^{Z+})$, shown in Table 4 were obtained. The volumes were determined from scans of the line intensities along the x axis and at right angles to it.

Table 4

| z | $N(C^{Z+})$ | K.E. joules |
|---|---|---|
| 6 | $0{\cdot}2 \times 10^{15}$ | 0·2 |
| 5 | 1·4 | 1·3 |
| 4 | 2·0 | 1·3 |
| 3 | 1·7 | 0·4 |
| 2 | 0·9 | 0·1 |
| Total | $6{\cdot}2 \times 10^{15}$ | 3·3 |
| | | |
| 1 | $< 7 \times 10^{15}$ | <0·3 |
| Total | $< 13 \times 10^{15}$ | <3·6 |

A summation of the numbers $N(C^{Z+})$ shows that the total number of carbon ions of all charges lies between 0·6 and $1{\cdot}3 \times 10^{16}$; the uncertainty being introduced by the uncertainty in the value $N(C^{1+})$. Errors principally in number densities are responsible for an additional uncertainty of ± 60% in the various totals.

## 6.7 The Calculation of the Plasma Energy

A multiplication of the total numbers of ions from Table 4 with the ion kinetic energies from Table 2 gives the total energies represented by the kinetic motion of the ions. These are shown in Table 4. A summation of these energies gives the result that the total energy represented by the kinetic velocities of all the ions is about 3·5 joules with an overall uncertainty of ± 70%. When the thermal energy of the electrons (~ 0·1 joules), the ionization energy (~0·2 joules) and the energy lost by radiation (negligible) is added to these figures, the total known energy possessed by the plasma is seen to be about 3·8 joules. This value may be compared with the initial laser energy of 5 joules. Thus the important conclusion may be drawn that about 75% of the initial laser energy is deposited in the plasma plume and almost all of this energy is in the form of the streaming velocity of the ions. The error in this estimation is as given above. Note that this and all errors in this paper are given in the spirit of 90% confidence limits.

## 6.8 The Momentum Balance of the Plasma Plume

It has been suggested (Afanasyev et al., 1966; Caruso et al., 1966) that the recoil from the momentum of the plasma plume is taken up by a shock wave which propagates into the target material in the same direction as the laser beam. In discussing the momentum balance it is useful to make use of some of the data acquired in an experiment that was being done concurrently with the present one and which has already been reported in the literature (Griffin and Schluter, 1968). In this other experiment which was performed with the same laser on polyethylene targets somewhat thinner than

those used for the spectroscopy, it was shown that for a given laser power there was a minimum target thickness for the majority of the power to be absorbed during the laser pulse. For thinner targets it was shown that while for the early part of the pulse there was almost complete absorption, towards the end of the pulse the beam burst through the target with only a small amount of absorption. A multiplication of the minimum target thickness for complete absorption with the area of the laser focal spot gives the total number of carbon atoms contained in the cylinder of target material with which the laser interacts directly during the period of the pulse. This number comes to $2{\cdot}4 \times 10^{17}$ and may be compared with the total number of carbon ions in the plasma plume, measured spectroscopically to be between 0·6 and $1{\cdot}3 \times 10^{16}$ particles. Thus of the total number of carbon atoms vaporised by the laser directly only 3 to 6% are ionized. By balancing the momentum of the recoil shock heated vapour against the momentum of the plasma jet, the energy recoil was determined to be 2 to 3·6 eV per carbon atom and the total recoil energy ·08 J to ·14 J. Gregg and Thomas, 1966, have reported the use of a ballistic pendulum to measure the recoil momentum produced by the plasma plume. The value that they find for a graphite target agrees within a factor two with the value obtained here from the spectroscopic measurements.

The exclusion of hydrogen ions from the above calculations is justified on the grounds of their small mass compared to that of the carbon ions.

## 7. Conclusion

This paper has described a spectroscopic study of a laser produced plasma. The observations included a photograph of the recombination continuum of carbon V and carbon VI taken with good space resolution to provide estimates of the electron temperature as a function of distance from the target. A monochromator in the visible and quartz ultraviolet region of the spectrum was used to make both time and space resolved measurements of absolute intensities of spectral lines. These were interpreted through the Saha-Boltzmann equation to give estimates of the plasma electron temperature, electron density, and densities and velocities of carbon ions having charge 1 to 6.

The main results of the paper are summarised in Table 5 where the distribution of energy expressed as a percentage of the incident laser energy, is given. In order to account for 100% of the incident energy it is necessary to conclude that almost 80% or more of the incident energy is converted to the kinetic energy of the ions.

Table 5

Energy distribution

| | |
|---|---|
| Reflected and transmitted (Schluter and Griffin, 1968): | 6 - 14% |
| Electron thermal energy: | ~ 2% |
| Ionization energy: | ~ 4% |
| Recoil energy: | 1·5 - 3% |
| Ion kinetic energies (excluded are $H^+$ ion and H and C atoms): | 20 - 100% |

Another result of the experiment by Griffin and Schluter 1968 has been carried over to the analysis of the present experiment. They were able to show that the laser beam interacts directly with about $2{\cdot}4 \times 10^{17}$ carbon atoms in the polyethylene target. In the present experiment it has been shown that only about $10^{16}$ or 4% are ionized. The rest of the target material must be present presumably in order to absorb the recoil from the plasma jet.

The experiment has also shown that as they expand out in the plasma plume the electrons cool adiabatically. This observation is consistent with a plasma model where the electron thermal energy is transferred to the ions during expansion.

## 8. Acknowledgements

We are grateful to Mr. J. Payne and Mr. R.J. Hutcheon for their assistance with the experiment and to Dr. A.H. Gabriel for his criticism of the manuscript.

## 9. REFERENCES

### General References (Introduction)


AMBARTSUMYAN, R.V., BASOV, N.G., BOIKO, V.A., ZNEV, V.S., KROKHIN, O.N., KRYUKOV, P.G., SEANT-SKII, Yu.V. and STOILOV, Yu. Yu., 1965, Zh. Eksp. Teor. Fiz., 48, 1583-8.

ARCHBOLD, E., HARPER, D.W. and HUGHES, T.P., 1964, Brit. J. of Appl. Phys., 15, 1321-6.

BASOV, N.G., BOIKO, V.A., DEMENTYEV, V.A., KROKHIN, O.N. and SKLIZKOV, G.V., 1966, Zh. Eksp. Teor. Fiz., 51, 989-1000.

BASOV, N.G., BOIKO, V.A., VOINOV, Yu.P., KONONOV, E.Ya., MANDELSHTAM, S.L. and SKLIZKOV, G.V., 1967, Zh. Eksp. Teor. Fiz. Pisma v Redaktsiyu, 5, 177-180.

BURGESS, D.D., FAWCETT, B.C. and PEACOCK, N.J., 1967, Proc. Phys. Soc., 92, 805-16.

DAVID, C., AVIZONIS, P.V., WEICHEL, H., BRUCE, C. and PYATT, K.D., 1966, I.E.E.E. J. of Quantum Electronics, QE-2, 493-9.

EHLER, A.W., 1966, J. of Appl. Phys., 37, 4962-6.

EHLER, A.W. and WEISSLER, G.L., 1965, Bull. Am. Phys. Soc., B, 10, p.1182.

EHLER, A.W. and WEISSLER, G.L., 1966, Appl. Phys. Letters, 8, 89-91.

FAWCETT, B.C., GABRIEL, A.H., IRONS, F.E., PEACOCK, N.J. and SAUNDERS, P.A.H., 1966, Proc. Phys. Soc., 88, 1051-3.

FAWCETT, B.C. and IRONS, F.E., 1966, Proc. Phys. Soc., 89, 1063-4.

FAWCETT, B.C., GABRIEL, A.H. and SAUNDERS, P.A.H., 1967, Proc. Phys. Soc., 90, 863-7.

FAWCETT, B.C., BURGESS, D.D. and PEACOCK, N.J., 1967, Proc. Phys. Soc., 91, 970-2.

FAWCETT, B.C. and PEACOCK, N.J., 1967, Proc. Phys. Soc., 91, 973-5.

GREGG, D.W. and THOMAS, S.J., 1966, J. of Appl. Phys., 37, 4313-6.

GREGG, D.W. and THOMAS, S.J., 1967, J. of Appl. Phys., 38, 1729-31.

HARRIS, T.J., 1963, I.B.M. J. of Research and Development, 7, 342-4.

LANGER, P., TONON, G., FLOUX, F. and DUCAUZE, A., 1966, I.E.E.E. J. of Quantum Electronics, QE-2, 499-507.

OPOWER, H. and PRESS, W., 1966, Z. Naturforschg., 21a, 344-50.

READY, J.F., 1963, Appl. Phys. Letters, 3, 11-13.

SUCOV, E.W., PACK, J.L., PHELPS, A.V. and ENGELHARDT, A.G., 1967, Phys. of Fluids, 10, 2035-48.

WEICHEL, H. and AVIZONIS, P.V., 1966, Appl. Phys. Letters, 9, 334-7.

Other references

AFANASYEV, Yu.V., KROKHIN, O.N., and SKLIZKOV, G.V., 1966, I.E.E.E. J. of Quantum Electronics, QE-2, 483-6.

BATES, D.R. and DAMGAARD, A., 1949, Phil. Trans. R. Soc., 242A, 101-22.

BATES, D.R., KINGSTON, A.E. and McWHIRTER, R.W.P., 1962, Proc. Roy. Soc., 267A, 297-312.

CARUSO, A., BERTOTTI, B. and GIUPPONI, P., 1966, Nuovo Cimento, 45B, 176-89.

COOPER, J., 1966, Reports on Progress in Physics, 29, 35-130.

ELWERT, G., 1954, Z. Naturforschg., 9a, 432-9.

GARCIA, J.D., and MACK, J.E., 1965, J. Opt. Soc. Amer. 55, 654-85.

GREGG, D.W. and THOMAS, S.J., 1966, J. of Appl. Phys., 37, 2787-9.

GRIFFIN, W.G. and SCHLUTER, J., 1968, Phys. Letters, 26A, 241-2.

MACKAY, R.C., POLLACK, S.A. and WITTE, R.S., 1965, Rev. of Sci. Instrum., 36, 1715-8.

McWHIRTER, R.W.P., 1965, Plasma Diagnostic Techniques, Eds., R.H. Huddlestone and S.L. Leonard (New York: Academic Press), chapter 5, pp.201-64.

McWHIRTER, R.W.P. and HEARN, A.G., 1963, Proc. Phys. Soc., 82, 641-54.

MORGAN, F.J., GABRIEL, A.H. and BARTON, M.J., 1968, to be published in J. of Sci. Instrum.,

WIESE, W.L., SMITH, M.W. and GLENNON, B.M., 1966, National Standard Reference Data Series, Report NSRDS-NBS4, Washington, 1, 1-152.

WILSON, R., 1962, J. Quant. Spectr. Radiative Transfer, 2, 477-90.

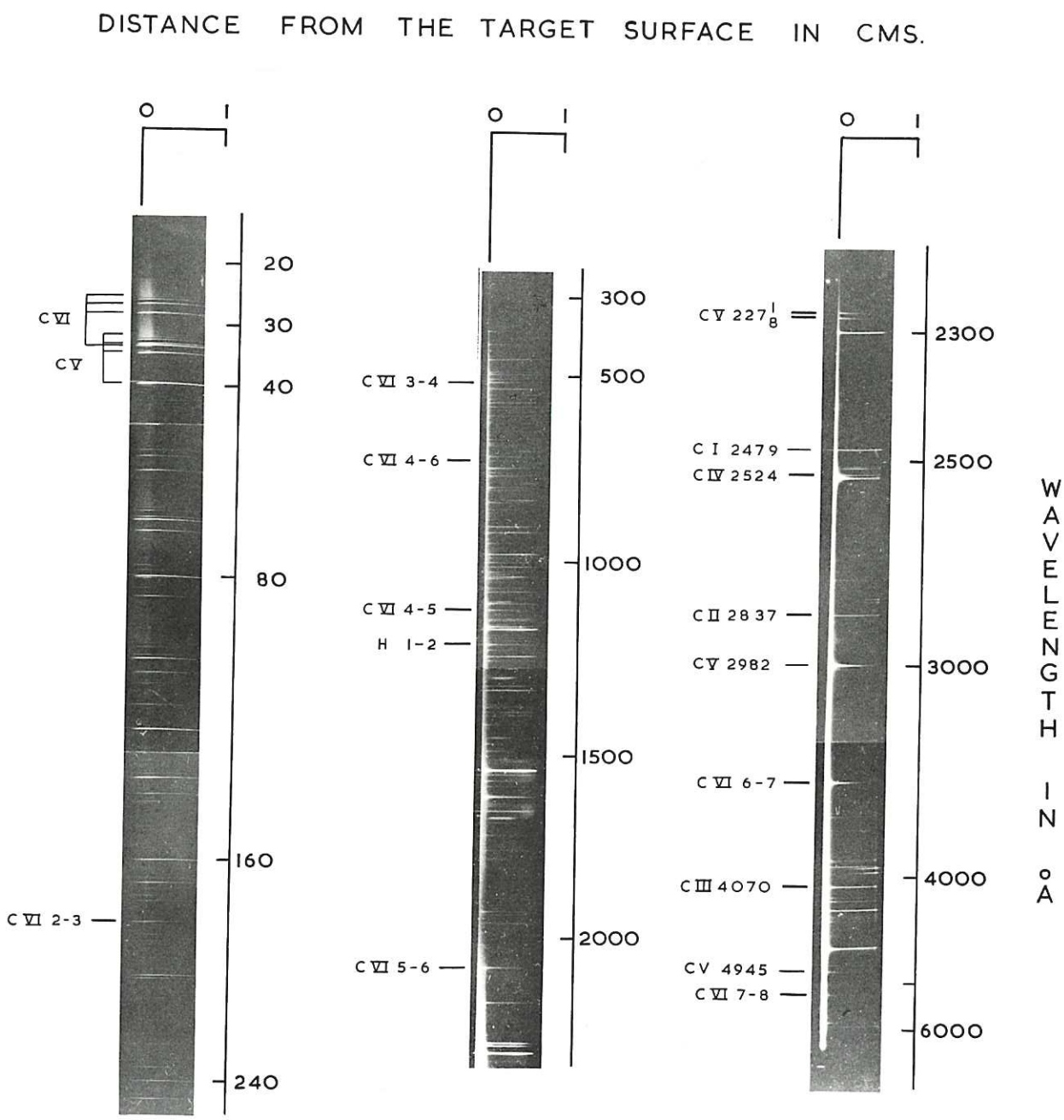


Fig. 1 (CLM-P 176)

Spectra, covering the range 20 Å to 6000 Å , of the plasma from a laser-irradiated polythene foil. Plasma expansion is from left to right

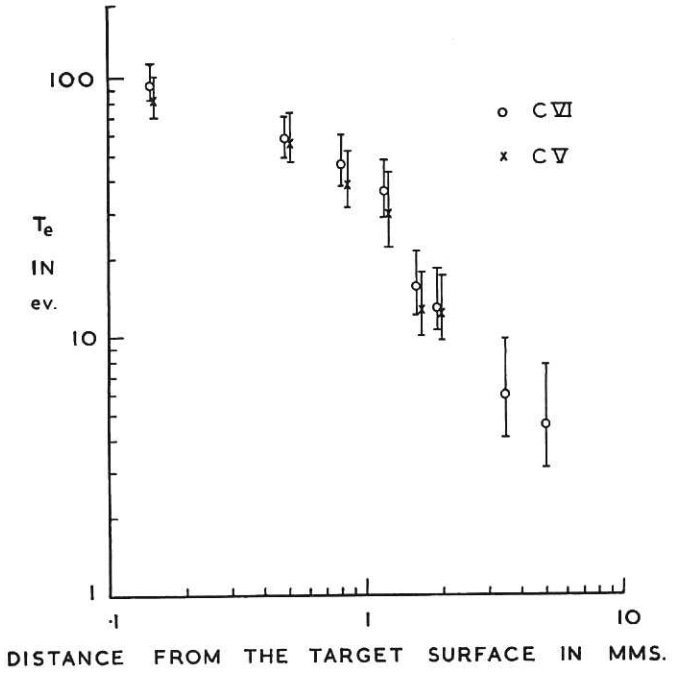


Fig. 2 (CLM-P 176)
Electron temperature as a function of distance

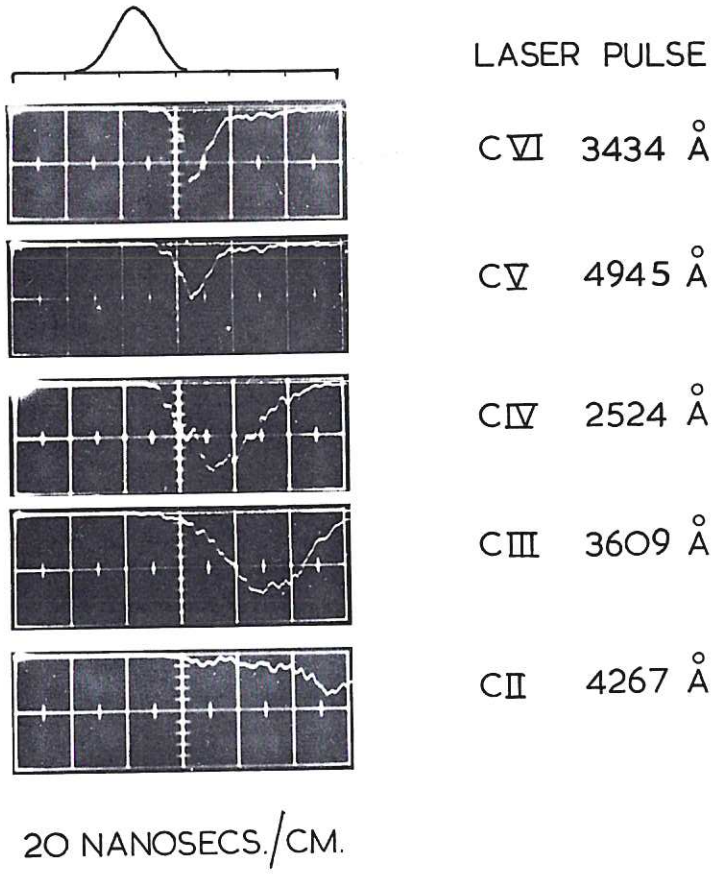


Fig. 3 (CLM-P 176)
Oscillograms of lines of C II-VI, 2 mm from the target surface

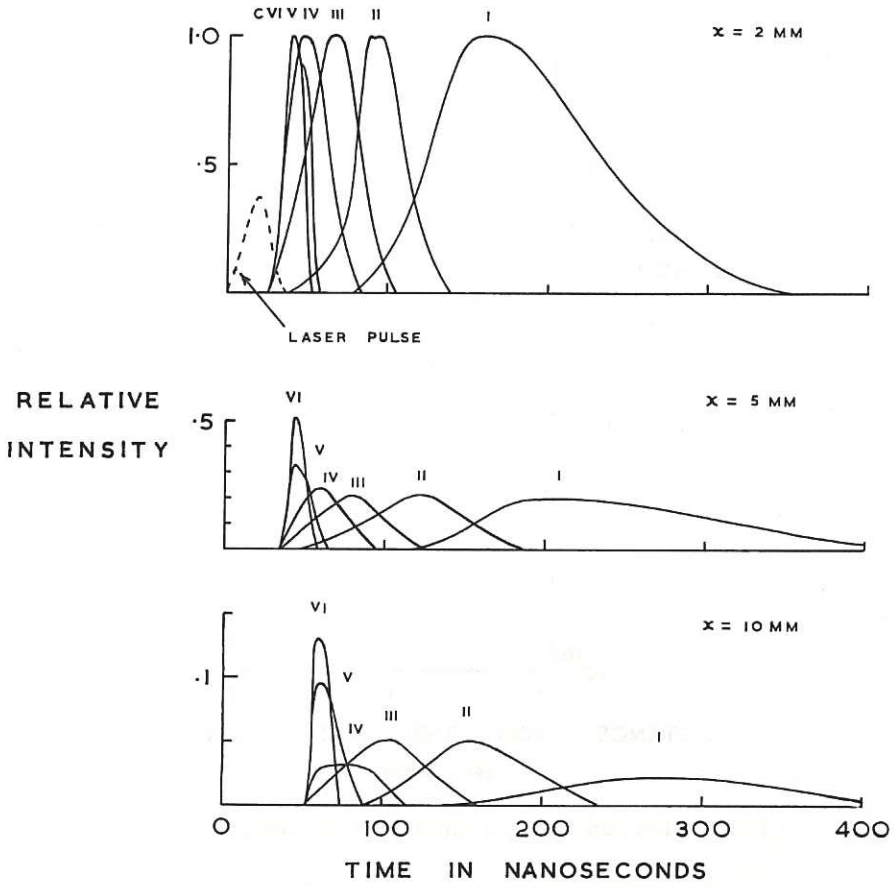


Fig. 4 Time variation of lines of C I - VI (CLM-P 176)

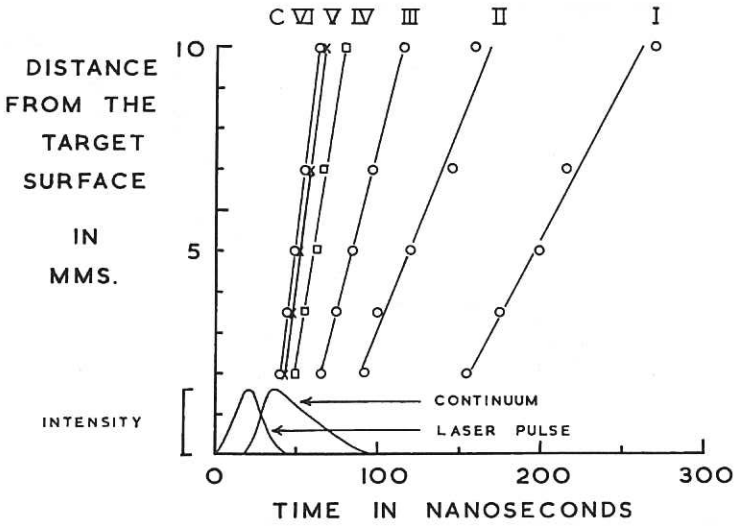


Fig. 5 (CLM-P 176)
Plot of distance versus time for the peak intensities of lines of C I - VI

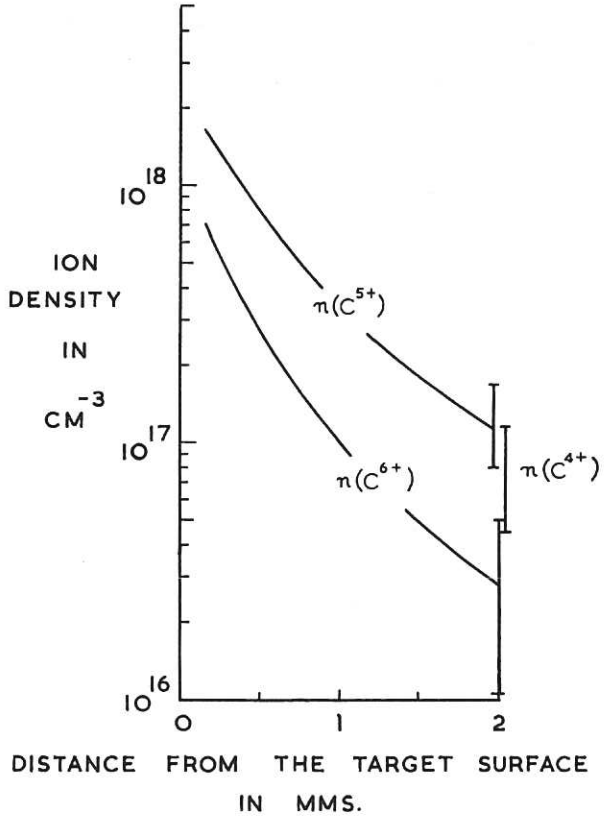


Fig. 6 Ion density as a function of distance (CLM-P176)

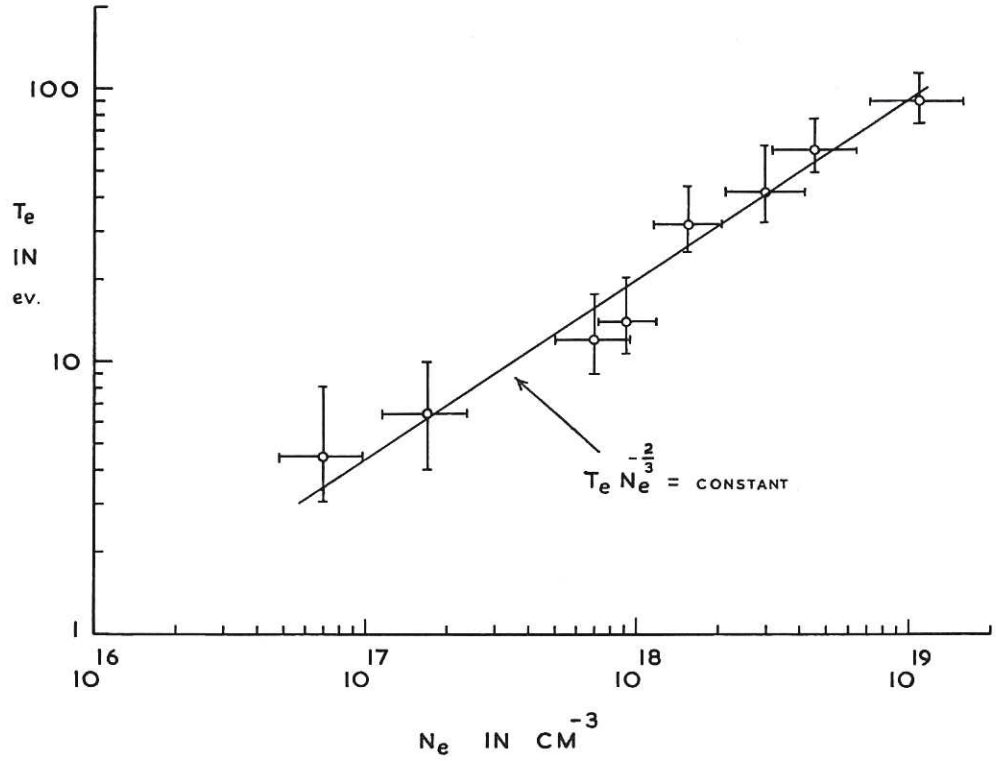


Fig. 7 (CLM-P176)
Electron temperature plotted as a function of electron density